Search for the decay B(0) -> gamma gamma

del Amo Sanchez, P.; Raven, H.G.; Snoek, H.; BaBar, Collaboration

published in
Physical Review D
2011

DOI (link to publisher)
10.1103/PhysRevD.83.032006

document version
Publisher's PDF, also known as Version of record

Search for the decay $B^0 \to \gamma\gamma$

P. del Amo Sanchez,[1] J. P. Lees,[1] V. Poireau,[1] E. Prencipe,[1] V. Tisserand,[1] J. Garra Tico,[2] E. Grauges,[2] M. Martinelli,[3a,3b] A. Palano,[3a,3b] M. Pappagallo,[3a,3b] G. Eigen,[4] B. Stugu,[4] L. Sun,[4] M. Battaglia,[5] D. N. Brown,[5] B. Hooberman,[5] L. T. Kerth,[5] Yu. G. Kolomensky,[5] G. Lynch,[5] I. L. Osipenkov,[5] T. Tanabe,[5] C. M. Hawkes,[6] A. T. Watson,[6] H. Koch,[7] T. Schroeder,[7] D. J. Asgeirsson,[8] C. Hearty,[8] T. S. Mattison,[8] J. A. McKenna,[8] A. Khan,[9] A. Randle-Conde,[9] V. E. Blinov,[10] A. R. Buzykaev,[10] V. P. Druzhinin,[10] V. B. Golubev,[10] A. P. Onuchin,[10] S. I. Serednyakov,[10] Yu. I. Skovpen,[10] E. P. Solodov,[10] K. Yu. Todyshev,[10] A. N. Yushkov,[10] M. Bondioli,[11] S. Curry,[11] D. Kirkby,[11] A. J. Lankford,[11] M. Mandelkern,[11] E. C. Martin,[11] D. P. Stoker,[11] H. Atmacan,[12] J. W. Gary,[12] F. Liu,[12] O. Long,[12] G. M. Vitug,[12] C. Campagnari,[13] T. M. Hong,[13] D. Kovalskyi,[13] J. D. Richman,[13] C. West,[13] A. M. Eisner,[14] C. A. Heusch,[14] J. Kroseberg,[14] W. S. Lockman,[14] A. J. Martinez,[14] T. Schalk,[14] B. A. Schumm,[14] A. Seiden,[14] L. O. Winstrom,[14] C. H. Cheng,[15] D. A. Doll,[15] B. Echenard,[15] D. G. Hitlin,[15] P. Ongmongkolkul,[15] F. C. Porter,[15] A. Y. Rakitin,[15] R. Andreassen,[16] M. S. Dubrovin,[16] G. Mancinelli,[16] B. T. Meadows,[16] M. D. Sokoloff,[16] P. C. Bloom,[17] W. T. Ford,[17] A. Gaz,[17] M. Nagel,[17] U. Nauenberg,[17] J. G. Smith,[17] S. R. Wagner,[17] R. Ayad,[18,*] W. H. Toki,[18] H. Jasper,[19] T. M. Karbach,[19] J. Merkel,[19] A. Petzold,[19] B. Spaan,[19] K. Wacker,[19] M. J. Kobel,[20] K. R. Schubert,[20] R. Schwierz,[20] D. Bernard,[21] M. Verderi,[21] P. J. Clark,[22] S. Playfer,[22] J. E. Watson,[22] M. Andreotti,[23a,23b] D. Bettoni,[23a] C. Bozzi,[23a] R. Calabrese,[23a,23b] A. Cecchi,[23a,23b] G. Cibinetto,[23a,23b] E. Fioravanti,[23a,23b] P. Franchini,[23a,23b] E. Luppi,[23a,23b] M. Munerato,[23a,23b] M. Negrini,[23a,23b] A. Petrella,[23a,23b] L. Piemontese,[23a] R. Baldini-Ferroli,[24] A. Calcaterra,[24] R. de Sangro,[24] G. Finocchiaro,[24] M. Nicolaci,[24] S. Pacetti,[24] P. Patteri,[24] I. M. Peruzzi,[24,†] M. Piccolo,[24] M. Rama,[24] A. Zallo,[24] R. Contri,[25a,25b] E. Guido,[25a,25b] M. Lo Vetere,[25a,25b] M. R. Monge,[25a,25b] S. Passaggio,[25a] C. Patrignani,[25a,25b] E. Robutti,[25a] S. Tosi,[25a,25b] B. Bhuyan,[26] V. Prasad,[26] C. L. Lee,[27] M. Morii,[27] A. Adametz,[28] J. Marks,[28] U. Uwer,[28] F. U. Bernlochner,[29] M. Ebert,[29] H. M. Lacker,[29] T. Lueck,[29] A. Volk,[29] P. D. Dauncey,[30] M. Tibbetts,[30] P. K. Behera,[31] U. Mallik,[31] C. Chen,[32] J. Cochran,[32] H. B. Crawley,[32] L. Dong,[32] W. T. Meyer,[32] S. Prell,[32] E. I. Rosenberg,[32] A. E. Rubin,[32] A. V. Gritsan,[33] Z. J. Guo,[33] N. Arnaud,[34] M. Davier,[34] D. Derkach,[34] J. Firmino da Costa,[34] G. Grosdidier,[34] F. Le Diberder,[34] A. M. Lutz,[34] B. Malaescu,[34] A. Perez,[34] P. Roudeau,[34] M. H. Schune,[34] J. Serrano,[34] V. Sordini,[34,‡] A. Stocchi,[34] L. Wang,[34] G. Wormser,[34] D. J. Lange,[35] D. M. Wright,[35] I. Bingham,[36] C. A. Chavez,[36] J. P. Coleman,[36] J. R. Fry,[36] E. Gabathuler,[36] R. Gamet,[36] D. E. Hutchcroft,[36] D. J. Payne,[36] C. Touramanis,[36] A. J. Bevan,[37] F. Di Lodovico,[37] R. Sacco,[37] M. Sigamani,[37] G. Cowan,[38] S. Paramesvaran,[38] A. C. Wren,[38] D. N. Brown,[39] C. L. Davis,[39] A. G. Denig,[40] M. Fritsch,[40] W. Gradl,[40] A. Hafner,[40] K. E. Alwyn,[41] D. Bailey,[41] R. J. Barlow,[41] G. Jackson,[41] G. D. Lafferty,[41] J. Anderson,[42] R. Cenci,[42] A. Jawahery,[42] D. A. Roberts,[42] G. Simi,[42] J. M. Tuggle,[42] C. Dallapiccola,[43] E. Salvati,[43] R. Cowan,[44] D. Dujmic,[44] G. Sciolla,[44] M. Zhao,[44] D. Lindemann,[45] P. M. Patel,[45] S. H. Robertson,[45] M. Schram,[45] P. Biassoni,[46a,46b] A. Lazzaro,[46a,46b] V. Lombardo,[46a] F. Palombo,[46a,46b] S. Stracka,[46a,46b] L. Cremaldi,[47] R. Godang,[47,§] R. Kroeger,[47] P. Sonnek,[47] D. J. Summers,[47] X. Nguyen,[48] M. Simard,[48] P. Taras,[48] G. De Nardo,[49a,49b] D. Monorchio,[49a,49b] G. Onorato,[49a,49b] C. Sciacca,[49a,49b] G. Raven,[50] H. L. Snoek,[50] C. P. Jessop,[51] K. J. Knoepfel,[51] J. M. LoSecco,[51] W. F. Wang,[51] L. A. Corwin,[52] K. Honscheid,[52] R. Kass,[52] J. P. Morris,[52] N. L. Blount,[53] J. Brau,[53] R. Frey,[53] O. Igonkina,[53] J. A. Kolb,[53] R. Rahmat,[53] N. B. Sinev,[53] D. Strom,[53] J. Strube,[53] E. Torrence,[53] G. Castelli,[54a,54b] E. Feltresi,[54a,54b] N. Gagliardi,[54a,54b] M. Margoni,[54a,54b] M. Morandin,[54a] M. Posocco,[54a] M. Rotondo,[54a] F. Simonetto,[54a,54b] R. Stroili,[54a,54b] E. Ben-Haim,[55] G. R. Bonneaud,[55] H. Briand,[55] G. Calderini,[55] J. Chauveau,[55] O. Hamon,[55] Ph. Leruste,[55] G. Marchiori,[55] J. Ocariz,[55] J. Prendki,[55] S. Sitt,[55] M. Biasini,[56a,56b] E. Manoni,[56a,56b] A. Rossi,[56a,56b] C. Angelini,[57a,57b] G. Batignani,[57a,57b] S. Bettarini,[57a,57b] M. Carpinelli,[57a,57b,‖] G. Casarosa,[57a,57b] A. Cervelli,[57a,57b] F. Forti,[57a,57b] M. A. Giorgi,[57a,57b] A. Lusiani,[57a,57c] N. Neri,[57a,57b] E. Paoloni,[57a,57b] G. Rizzo,[57a,57b] J. J. Walsh,[57a] D. Lopes Lopes Pegna,[58] C. Lu,[58] J. Olsen,[58] A. J. S. Smith,[58] A. V. Telnov,[58] F. Anulli,[59a] E. Baracchini,[59a,59b] G. Cavoto,[59a] R. Faccini,[59a,59b] F. Ferrarotto,[59a] F. Ferroni,[59a,59b] M. Gaspero,[59a,59b] L. Li Gioi,[59a] M. A. Mazzoni,[59a] G. Piredda,[59a] F. Renga,[59a,59b] T. Hartmann,[60] T. Leddig,[60] H. Schröder,[60] R. Waldi,[60] T. Adye,[61] B. Franek,[61] E. O. Olaiya,[61] F. F. Wilson,[61] S. Emery,[62] G. Hamel de Monchenault,[62] G. Vasseur,[62] Ch. Yèche,[62] M. Zito,[62] M. T. Allen,[63] D. Aston,[63] D. J. Bard,[63] R. Bartoldus,[63] J. F. Benitez,[63] C. Cartaro,[63] M. R. Convery,[63] J. Dorfan,[63] G. P. Dubois-Felsmann,[63] W. Dunwoodie,[63] R. C. Field,[63] M. Franco Sevilla,[63] B. G. Fulsom,[63] A. M. Gabareen,[63] M. T. Graham,[63] P. Grenier,[63] C. Hast,[63] W. R. Innes,[63] M. H. Kelsey,[63] H. Kim,[63] P. Kim,[63] M. L. Kocian,[63] D. W. G. S. Leith,[63] S. Li,[63] B. Lindquist,[63] S. Luitz,[63] V. Luth,[63] H. L. Lynch,[63] D. B. MacFarlane,[63] H. Marsiske,[63] D. R. Muller,[63] H. Neal,[63]

S. Nelson,[63] C. P. O'Grady,[63] I. Ofte,[63] M. Perl,[63] T. Pulliam,[63] B. N. Ratcliff,[63] A. Roodman,[63] A. A. Salnikov,[63] V. Santoro,[63] R. H. Schindler,[63] J. Schwiening,[63] A. Snyder,[63] D. Su,[63] M. K. Sullivan,[63] S. Sun,[63] K. Suzuki,[63] J. M. Thompson,[63] J. Va'vra,[63] A. P. Wagner,[63] M. Weaver,[63] C. A. West,[63] W. J. Wisniewski,[63] M. Wittgen,[63] D. H. Wright,[63] H. W. Wulsin,[63] A. K. Yarritu,[63] C. C. Young,[63] V. Ziegler,[63] X. R. Chen,[64] W. Park,[64] M. V. Purohit,[64] R. M. White,[64] J. R. Wilson,[64] S. J. Sekula,[65] M. Bellis,[66] P. R. Burchat,[66] A. J. Edwards,[66] T. S. Miyashita,[66] S. Ahmed,[67] M. S. Alam,[67] J. A. Ernst,[67] B. Pan,[67] M. A. Saeed,[67] S. B. Zain,[67] N. Guttman,[68] A. Soffer,[68] P. Lund,[69] S. M. Spanier,[69] R. Eckmann,[70] J. L. Ritchie,[70] A. M. Ruland,[70] C. J. Schilling,[70] R. F. Schwitters,[70] B. C. Wray,[70] J. M. Izen,[71] X. C. Lou,[71] F. Bianchi,[72a,72b] D. Gamba,[72a,72b] M. Pelliccioni,[72a,72b] M. Bomben,[73a,73b] L. Lanceri,[73a,73b] L. Vitale,[73a,73b] N. Lopez-March,[74] F. Martinez-Vidal,[74] D. A. Milanes,[74] A. Oyanguren,[74] J. Albert,[75] Sw. Banerjee,[75] H. H. F. Choi,[75] K. Hamano,[75] G. J. King,[75] R. Kowalewski,[75] M. J. Lewczuk,[75] I. M. Nugent,[75] J. M. Roney,[75] R. J. Sobie,[75] T. J. Gershon,[76] P. F. Harrison,[76] T. E. Latham,[76] E. M. T. Puccio,[76] H. R. Band,[77] S. Dasu,[77] K. T. Flood,[77] Y. Pan,[77] R. Prepost,[77] C. O. Vuosalo,[77] and S. L. Wu[77]

(*BABAR* Collaboration)

[1]*Laboratoire d'Annecy-le-Vieux de Physique des Particules (LAPP), Université de Savoie, CNRS/IN2P3, F-74941 Annecy-Le-Vieux, France*
[2]*Universitat de Barcelona, Facultat de Fisica, Departament ECM, E-08028 Barcelona, Spain*
[3a]*INFN Sezione di Bari, I-70126 Bari, Italy*
[3b]*Dipartimento di Fisica, Università di Bari, I-70126 Bari, Italy*
[4]*University of Bergen, Institute of Physics, N-5007 Bergen, Norway*
[5]*Lawrence Berkeley National Laboratory and University of California, Berkeley, California 94720, USA*
[6]*University of Birmingham, Birmingham, B15 2TT, United Kingdom*
[7]*Ruhr Universität Bochum, Institut für Experimentalphysik 1, D-44780 Bochum, Germany*
[8]*University of British Columbia, Vancouver, British Columbia, Canada V6T 1Z1*
[9]*Brunel University, Uxbridge, Middlesex UB8 3PH, United Kingdom*
[10]*Budker Institute of Nuclear Physics, Novosibirsk 630090, Russia*
[11]*University of California at Irvine, Irvine, California 92697, USA*
[12]*University of California at Riverside, Riverside, California 92521, USA*
[13]*University of California at Santa Barbara, Santa Barbara, California 93106, USA*
[14]*University of California at Santa Cruz, Institute for Particle Physics, Santa Cruz, California 95064, USA*
[15]*California Institute of Technology, Pasadena, California 91125, USA*
[16]*University of Cincinnati, Cincinnati, Ohio 45221, USA*
[17]*University of Colorado, Boulder, Colorado 80309, USA*
[18]*Colorado State University, Fort Collins, Colorado 80523, USA*
[19]*Technische Universität Dortmund, Fakultät Physik, D-44221 Dortmund, Germany*
[20]*Technische Universität Dresden, Institut für Kern- und Teilchenphysik, D-01062 Dresden, Germany*
[21]*Laboratoire Leprince-Ringuet, CNRS/IN2P3, Ecole Polytechnique, F-91128 Palaiseau, France*
[22]*University of Edinburgh, Edinburgh EH9 3JZ, United Kingdom*
[23a]*INFN Sezione di Ferrara, I-44100 Ferrara, Italy*
[23b]*Dipartimento di Fisica, Università di Ferrara, I-44100 Ferrara, Italy*
[24]*INFN Laboratori Nazionali di Frascati, I-00044 Frascati, Italy*
[25a]*INFN Sezione di Genova, I-16146 Genova, Italy*
[25b]*Dipartimento di Fisica, Università di Genova, I-16146 Genova, Italy*
[26]*Indian Institute of Technology Guwahati, Guwahati, Assam, 781 039, India*
[27]*Harvard University, Cambridge, Massachusetts 02138, USA*
[28]*Universität Heidelberg, Physikalisches Institut, Philosophenweg 12, D-69120 Heidelberg, Germany*
[29]*Humboldt-Universität zu Berlin, Institut für Physik, Newtonstr. 15, D-12489 Berlin, Germany*
[30]*Imperial College London, London, SW7 2AZ, United Kingdom*
[31]*University of Iowa, Iowa City, Iowa 52242, USA*
[32]*Iowa State University, Ames, Iowa 50011-3160, USA*
[33]*Johns Hopkins University, Baltimore, Maryland 21218, USA*
[34]*Laboratoire de l'Accélérateur Linéaire, IN2P3/CNRS et Université Paris-Sud 11, Centre Scientifique d'Orsay, B. P. 34, F-91898 Orsay Cedex, France*
[35]*Lawrence Livermore National Laboratory, Livermore, California 94550, USA*
[36]*University of Liverpool, Liverpool L69 7ZE, United Kingdom*
[37]*Queen Mary, University of London, London, E1 4NS, United Kingdom*
[38]*University of London, Royal Holloway and Bedford New College, Egham, Surrey TW20 0EX, United Kingdom*

[39]*University of Louisville, Louisville, Kentucky 40292, USA*
[40]*Johannes Gutenberg-Universität Mainz, Institut für Kernphysik, D-55099 Mainz, Germany*
[41]*University of Manchester, Manchester M13 9PL, United Kingdom*
[42]*University of Maryland, College Park, Maryland 20742, USA*
[43]*University of Massachusetts, Amherst, Massachusetts 01003, USA*
[44]*Massachusetts Institute of Technology, Laboratory for Nuclear Science, Cambridge, Massachusetts 02139, USA*
[45]*McGill University, Montréal, Québec, Canada H3A 2T8*
[46a]*INFN Sezione di Milano, I-20133 Milano, Italy*
[46b]*Dipartimento di Fisica, Università di Milano, I-20133 Milano, Italy*
[47]*University of Mississippi, University, Mississippi 38677, USA*
[48]*Université de Montréal, Physique des Particules, Montréal, Québec, Canada H3C 3J7*
[49a]*INFN Sezione di Napoli, I-80126 Napoli, Italy*
[49b]*Dipartimento di Scienze Fisiche, Università di Napoli Federico II, I-80126 Napoli, Italy*
[50]*NIKHEF, National Institute for Nuclear Physics and High Energy Physics, NL-1009 DB Amsterdam, The Netherlands*
[51]*University of Notre Dame, Notre Dame, Indiana 46556, USA*
[52]*Ohio State University, Columbus, Ohio 43210, USA*
[53]*University of Oregon, Eugene, Oregon 97403, USA*
[54a]*INFN Sezione di Padova, I-35131 Padova, Italy*
[54b]*Dipartimento di Fisica, Università di Padova, I-35131 Padova, Italy*
[55]*Laboratoire de Physique Nucléaire et de Hautes Energies, IN2P3/CNRS, Université Pierre et Marie Curie-Paris6, Université Denis Diderot-Paris7, F-75252 Paris, France*
[56a]*INFN Sezione di Perugia, I-06100 Perugia, Italy*
[56b]*Dipartimento di Fisica, Università di Perugia, I-06100 Perugia, Italy*
[57a]*INFN Sezione di Pisa, I-56127 Pisa, Italy*
[57b]*Dipartimento di Fisica, Università di Pisa, I-56127 Pisa, Italy*
[57c]*Scuola Normale Superiore di Pisa, I-56127 Pisa, Italy*
[58]*Princeton University, Princeton, New Jersey 08544, USA*
[59a]*INFN Sezione di Roma, I-00185 Roma, Italy*
[59b]*Dipartimento di Fisica, Università di Roma La Sapienza, I-00185 Roma, Italy*
[60]*Universität Rostock, D-18051 Rostock, Germany*
[61]*Rutherford Appleton Laboratory, Chilton, Didcot, Oxon, OX11 0QX, United Kingdom*
[62]*CEA, Irfu, SPP, Centre de Saclay, F-91191 Gif-sur-Yvette, France*
[63]*SLAC National Accelerator Laboratory, Stanford, California 94309 USA*
[64]*University of South Carolina, Columbia, South Carolina 29208, USA*
[65]*Southern Methodist University, Dallas, Texas 75275, USA*
[66]*Stanford University, Stanford, California 94305-4060, USA*
[67]*State University of New York, Albany, New York 12222, USA*
[68]*Tel Aviv University, School of Physics and Astronomy, Tel Aviv, 69978, Israel*
[69]*University of Tennessee, Knoxville, Tennessee 37996, USA*
[70]*University of Texas at Austin, Austin, Texas 78712, USA*
[71]*University of Texas at Dallas, Richardson, Texas 75083, USA*
[72a]*INFN Sezione di Torino, I-10125 Torino, Italy*
[72b]*Dipartimento di Fisica Sperimentale, Università di Torino, I-10125 Torino, Italy*
[73a]*INFN Sezione di Trieste, I-34127 Trieste, Italy*
[73b]*Dipartimento di Fisica, Università di Trieste, I-34127 Trieste, Italy*
[74]*IFIC, Universitat de Valencia-CSIC, E-46071 Valencia, Spain*
[75]*University of Victoria, Victoria, British Columbia, Canada V8W 3P6*
[76]*Department of Physics, University of Warwick, Coventry CV4 7AL, United Kingdom*
[77]*University of Wisconsin, Madison, Wisconsin 53706, USA*
(Received 11 October 2010; published 7 February 2011)

We report the result of a search for the rare decay $B^0 \to \gamma\gamma$ in 426 fb^{-1} of data, corresponding to 226×10^6 $B^0\bar{B}^0$ pairs, collected on the $\Upsilon(4S)$ resonance at the PEP-II asymmetric-energy e^+e^- collider using the *BABAR* detector. We use a maximum likelihood fit to extract the signal yield and observe 21^{+13}_{-12} signal events with a statistical significance of 1.8σ. This corresponds to a branching fraction

*Present address: Temple University, Philadelphia, Pennsylvania 19122, USA
†Also at Università di Perugia, Dipartimento di Fisica, Perugia, Italy
‡Also at Università di Roma La Sapienza, I-00185 Roma, Italy
§Present address: University of South Alabama, Mobile, Alabama 36688, USA
‖Also at Università di Sassari, Sassari, Italy

$\mathcal{B}(B^0 \to \gamma\gamma) = (1.7 \pm 1.1(\text{stat.}) \pm 0.2(\text{syst.})) \times 10^{-7}$. Based on this result, we set a 90% confidence level upper limit of $\mathcal{B}(B^0 \to \gamma\gamma) < 3.2 \times 10^{-7}$.

DOI: 10.1103/PhysRevD.83.032006 PACS numbers: 13.20.He

I. INTRODUCTION

In the standard model (SM), the decay $B^0 \to \gamma\gamma$ occurs through a flavor-changing neutral current (FCNC) transition involving electroweak loop diagrams, as illustrated in Fig. 1. The decays $B^0 \to \gamma\gamma$ and $B_s \to \gamma\gamma$ are closely related, with the $b \to d\gamma\gamma$ transition being suppressed with respect to $b \to s\gamma\gamma$ by Cabbibo-Kobayashi-Maskawa (CKM) factors ($|V_{td}|^2/|V_{ts}|^2 \sim 0.04$). Hadron dynamics introduces uncertainties into the prediction of branching fractions for these decays and may modify the ratio away from the CKM-implied value. While $B^0 \to \gamma\gamma$ is expected to have a smaller branching fraction than $B_s \to \gamma\gamma$, a search for the latter faces the experimental challenge of obtaining a large sample of B_s mesons, whereas large samples of B^0 mesons are readily available from B Factory experiments running on the $\Upsilon(4S)$ resonance.

A leading-order calculation for the branching fraction of $B^0 \to \gamma\gamma$ yields an estimate of $(3.1^{+6.4}_{-1.6}) \times 10^{-8}$ [1]. This mode is sensitive to new physics that could lead to an enhancement of the branching fraction due to possible contributions of non-SM heavy particles occurring in the loop of the leading-order Feynman diagrams. Such enhancements to the branching fraction for $B^0 \to \gamma\gamma$ are less constrained than those for $B_s \to \gamma\gamma$ due to the fact that the $b \to s\gamma$ transition, responsible for $B_s \to \gamma\gamma$, is known much more accurately than $b \to d\gamma$. For example, some new physics scenarios involving an extended Higgs sector may considerably enhance the branching fractions with respect to the SM expectation [2]. Supersymmetry with broken R parity [3] also provides scenarios where order of magnitude enhancements are possible. In addition, since the two-photon final state can be either CP even or CP odd, studies of CP-violating effects may ultimately be possible.

The best previous upper limit on the branching fraction at 90% confidence level (CL) is $\mathcal{B}(B^0 \to \gamma\gamma) < 6.2 \times 10^{-7}$ set by the Belle experiment [4] using a data set recorded at the $\Upsilon(4S)$ resonance with an integrated luminosity of 104 fb^{-1}. For the related process $B_s \to \gamma\gamma$, Belle has set an upper limit on the branching fraction of 8.7×10^{-6} (90% CL) based on 23.6 fb^{-1} of data taken on the $\Upsilon(5S)$ resonance [5].

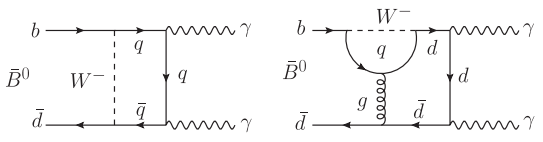

FIG. 1. Examples of lowest order SM Feynman diagrams for $B^0 \to \gamma\gamma$. The symbol q represents a u, c, or t quark. In some new physics scenarios, the W boson may be replaced by a charged Higgs particle.

We report herein a new search for the decay $B^0 \to \gamma\gamma$ which uses a data sample with integrated luminosity of 426 fb^{-1} taken at the $\Upsilon(4S)$ resonance. This corresponds to the entire *BABAR* $\Upsilon(4S)$ data set and contains 226×10^6 $B^0\bar{B}^0$ pairs. The analysis does not distinguish between B^0 and $\bar{B}^0$, and throughout this article, charge conjugation is implied for all reactions.

The analysis proceeds through several steps. The full data set is first reduced to a manageable size by selecting events based on loose kinematic criteria consistent with the $B^0 \to \gamma\gamma$ hypothesis. Studies are then performed to determine an optimal set of event selection criteria to maximize the efficiency for detecting $B^0 \to \gamma\gamma$ events while effectively rejecting background events. This analysis is performed "blind" in the sense that the event selection criteria are determined without considering the on-resonance data within a specific signal region, as defined below. We use an unbinned extended maximum likelihood fit to extract the signal yield from the remaining events. Finally, since no statistically significant $B^0 \to \gamma\gamma$ signal is observed, an upper limit on the branching fraction is calculated based on the likelihood function determined from the fit.

Section II of this article describes the *BABAR* detector and the $\Upsilon(4S)$ data set. Section III outlines the optimization of the event selection criteria and discusses backgrounds due to exclusive B decays. Section IV describes the fit methodology and Sec. V discusses the sources of systematic uncertainties. Finally, Sec. VI reports the resulting branching fraction and the upper limit.

II. THE *BABAR* DETECTOR AND DATA SET

The *BABAR* detector recorded data from the PEP-II B Factory located at the SLAC National Accelerator Laboratory. In PEP-II, head-on collisions of 9.0 GeV electrons and 3.1 GeV positrons provide a center-of-mass (CM) energy of 10.58 GeV that lies at the peak of the $\Upsilon(4S)$ resonance. The $\Upsilon(4S)$ meson decays almost exclusively to $B\bar{B}$ pairs. The subsequent B meson decays were observed in the *BABAR* detector, which has been described in detail elsewhere [6]. Briefly, a superconducting solenoid produces a 1.5 T magnetic field approximately parallel to the colliding electron and positron beams. Most detector subsystems are inside the volume of the solenoid. Charged particle tracking is accomplished by a combination of a five layer double-sided silicon strip vertex detector and a 40 layer drift chamber. The track reconstruction algorithm accepts tracks with a transverse momentum greater than

50 MeV/c. Identification of charged particles is accomplished using a ring-imaging Cherenkov detector augmented with energy loss measurements in the tracking detectors. Photons are detected in the electromagnetic calorimeter (EMC), which consists of 6580 CsI(Tl) crystals, oriented in a quasiprojective geometry with respect to the interaction point. Outside of the solenoid, the steel flux return is instrumented with a combination of resistive-plate chambers and limited streamer tubes to provide detection of muons and long-lived neutral hadrons.

The EMC is the most important detector subsystem for the $B^0 \to \gamma\gamma$ search. It provides polar angle coverage in the laboratory frame from 15.8° to 141.8°, and full azimuthal coverage, corresponding to a solid-angle coverage of 90% in the $\Upsilon(4S)$ CM frame. When a photon interacts with the EMC it creates an electromagnetic shower depositing its energy into many contiguous crystals, typically 10 to 30, hereafter called a ''cluster''. If no track in the event points to the cluster, it is designated as a photon candidate. Individual crystals are read out by a pair of silicon PIN photodiodes attached to the rear face of the crystal. Amplified signals are sampled and digitized with a period of 270 ns, providing a continuous data stream to which gain and pedestal corrections are applied. When a first level trigger is recorded, data samples in a time window of ± 1 μs are selected, producing a waveform which is analyzed by a feature extraction algorithm running in real time in readout modules. For events passing a higher level trigger, any EMC signal with energy above a 0.5 MeV threshold has its deposited energy and timing information recorded for offline analysis.

The energy resolution of the EMC is parameterized as the sum of two terms added in quadrature, given by [7]

$$\frac{\sigma_E}{E} = \frac{2.30\%}{\sqrt[4]{E\ (\mathrm{GeV})}} \oplus 1.35\%,$$

while the angular resolution in the polar angle θ and the azimuthal angle ϕ is given by

$$\sigma_\theta = \sigma_\phi = \frac{4.16}{\sqrt{E\ (\mathrm{GeV})}}\ \mathrm{mrad}.$$

In addition to the on-resonance data, a data sample of 44 fb^{-1} taken about 40 MeV below the $\Upsilon(4S)$ peak is recorded and used to validate the Monte Carlo (MC) simulation of continuum processes, $e^+e^- \to q\bar{q}$ ($q = u$, d, s, or c) and $e^+e^- \to \tau^+\tau^-$. MC simulated events are produced using the EVTGEN [8] package to model the physics of B meson decays and JETSET [9] to model quark fragmentation. The GEANT4 toolkit [10] is used to simulate the interaction of these events with the detector model. These tools are designed to take into account the varying detector and beam conditions encountered during data-taking. The MC events were analyzed with the same reconstruction algorithms, event selection and fitting procedures as data. MC samples of $B\bar{B}$ events correspond to about 4 times the integrated luminosity of the data. Those for $e^+e^- \to c\bar{c}$ events correspond to twice the data luminosity, while those for $e^+e^- \to u\bar{u}$, $d\bar{d}$, $s\bar{s}$ or $\tau^+\tau^-$ correspond to approximately the same luminosity as data. In addition, special MC data sets are created in which large samples of rare B meson decays are generated for the purpose of investigating the signal $B^0 \to \gamma\gamma$ decay as well as possible backgrounds due to other B decays.

III. EVENT SELECTION AND BACKGROUNDS

A. Event selection

The full $\Upsilon(4S)$ on-resonance data set is first reduced by selecting events that contain at least two photons with energies of $1.15 \le E^*_\gamma \le 3.50$ GeV, where the asterisk indicates a quantity in the $\Upsilon(4S)$ CM frame. We consider all combinations of two photons whose energies lie in this range and add their four-momentum to create B meson candidates. Hereafter, these photons are referred to as B candidate photons. The distribution of correctly reconstructed B candidates will peak in two nearly uncorrelated variables, m_{ES} and ΔE. The beam energy substituted mass is defined as $m_{\mathrm{ES}} \equiv \sqrt{E^{*2}_{\mathrm{beam}} - c^2\vec{p}^{\,*2}_B}/c^2$ and the energy difference is $\Delta E \equiv E^*_B - E^*_{\mathrm{beam}}$, where E^*_{beam} is the beam energy, and $\vec{p}^{\,*}_B$ and E^*_B are the three-momentum and energy of the B candidate, respectively. For $B^0 \to \gamma\gamma$ events, the m_{ES} distribution will peak at the B meson mass, 5.279 GeV/c^2 [11]. The MC predicts a full-width at half maximum (FWHM) of 6.5 MeV/c^2. The ΔE distribution is asymmetric and will peak near zero with a tail to the negative ΔE side due to photon energy loss outside the active volume of the EMC. The FWHM for ΔE predicted by the MC is about 150 MeV. We select an event for further analysis if it contains exactly one B candidate with $m_{\mathrm{ES}} > 5.1$ GeV/c^2 and $-0.50 \le \Delta E \le 0.50$ GeV. We find that in $B^0 \to \gamma\gamma$ MC only 0.06% of events have more than one B candidate and are removed by this selection. Some initial suppression of events produced from continuum processes, $e^+e^- \to q\bar{q}$ and $\tau^+\tau^-$, is achieved by requiring the ratio of the second-to-zeroth Fox-Wolfram moments [12], R_2, to be less than 0.90. This ratio is calculated from the momenta of all charged and neutral particles in the event. To suppress backgrounds from $e^+e^- \to \tau^+\tau^-$ events, which tend to have lower multiplicity compared to $B^0 \to \gamma\gamma$ events, the number of reconstructed charged tracks in the event is required to be greater than two.

We define a signal region in the m_{ES}-ΔE plane by fitting each variable in $B^0 \to \gamma\gamma$ MC and selecting a range around the peak of the distribution. The m_{ES} distribution is fit with a Crystal Ball (CB) shape [13] and we take a $\pm 3\sigma$ region around the CB peak corresponding to $5.27 \le m_{\mathrm{ES}} \le 5.29$ GeV/c^2. The ΔE distribution is parameterized using a double-sided modified Gaussian with tail parameters given by

$$f(\Delta E) \propto \exp\left(\frac{-(\Delta E-\mu)^2}{2\sigma_{L,R}^2+\alpha_{L,R}(\Delta E-\mu)^2}\right), \quad (1)$$

where μ is the peak of the ΔE distribution, $\sigma_{L,R}$ are the distribution widths, and $\alpha_{L,R}$ are tail parameters on the left and right side of the peak, respectively. We again take a $\pm 3\sigma$ interval around the peak corresponding to $-0.30 \leq \Delta E \leq 0.13$ GeV. This region is blinded in the on-resonance data until the maximum likelihood fit is performed. With this definition of the signal region, an $m_{\rm ES}$ sideband region is defined as $5.20 < m_{\rm ES} < 5.27$ GeV$/c^2$, and lower and upper ΔE sidebands are defined as $-0.50 \leq \Delta E < -0.30$ GeV and $0.13 < \Delta E \leq 0.50$ GeV, respectively.

We select photon candidates according to criteria chosen to remove poorly reconstructed photons. The energy of the cluster must be spread over at least 10 crystals with all crystals in the cluster having active electronics with correct calibrations. The shape of the cluster must be consistent with that of a photon in the defined energy range; we therefore require clusters to have lateral moments [14] in the range $0.15 \geq f_L \geq 0.50$. To ensure the shower is fully contained within the EMC volume, only photons whose polar angle is in the range $22.9^\circ < p_\theta < 137.5^\circ$ are selected. The photons are kept for further analysis if they are isolated from all other clusters in the event by at least 25 cm.

If an e^+e^- collision that results in a trigger is accompanied by another e^+e^- collision nearby in time, EMC signals from the out-of-time collision may populate the event of interest. Because of the large Bhabha-scattering cross section, these "pileup" events often involve high-energy electrons which may produce EMC clusters. Since the tracking detectors are sensitive over a narrower time window, electron-induced tracks may not point to the EMC clusters, causing them to be treated as photon candidates. If their energy is also measured incorrectly, artificial $B^0 \to \gamma\gamma$ candidates may result. This scenario is effectively rejected by requiring the total event energy to be less than 15.0 GeV and the cluster time of each B candidate photon to be consistent with the trigger event time.

The dominant source of backgrounds are photons produced from high-energy π^0 and η decays in continuum events. These events are suppressed using a likelihood ratio rejection technique. Each B candidate photon is separately combined with all other photons in the event and the invariant mass, $m_{\gamma\gamma'}$, and energy of the other photon, $E_{\gamma'}$, are used to calculate a likelihood ratio given by

$$L_i = \frac{P_i(m_{\gamma\gamma'}, E_{\gamma'})}{P_{\rm sig}(m_{\gamma\gamma'}, E_{\gamma'}) + P_i(m_{\gamma\gamma'}, E_{\gamma'})}. \quad (2)$$

In this equation, i is a label for π^0 or η, and P represents a two-dimensional probability density function (PDF). For each B candidate photon the pairing that gives the largest value of the likelihood ratio is assigned. The signal PDF, $P_{\rm sig}$, is constructed using simulated $B^0\bar{B}^0$ events containing a $B^0 \to \gamma\gamma$ decay where all B candidate photon pairings are used. The PDF for a π^0 or η, P_i, is constructed from simulated $e^+e^- \to q\bar{q}$ and $e^+e^- \to \tau^+\tau^-$ events. The B candidate photon in this case is required to be produced from a π^0 or η decay, while the other photon daughter is required to be reconstructed in the calorimeter. The energy of the other photon and the invariant mass of the pair are then used to construct the π^0 and η PDFs. A likelihood ratio near 1.0 (0.0) is consistent with the B candidate photon originating from a π^0 or η (signal B). Figure 2 shows the L_{π^0} and L_η distributions for $B^0 \to \gamma\gamma$ MC events and for B candidate photons from π^0 and η decays in MC continuum background events.

For high-energy π^0 decays with $E_{\pi^0} \gtrsim 2$ GeV, the daughter photons may not be separated enough in the EMC to be resolved individually. In this case the photon clusters are said to be "merged". A merged π^0 can mimic a B candidate photon because the cluster will have the full

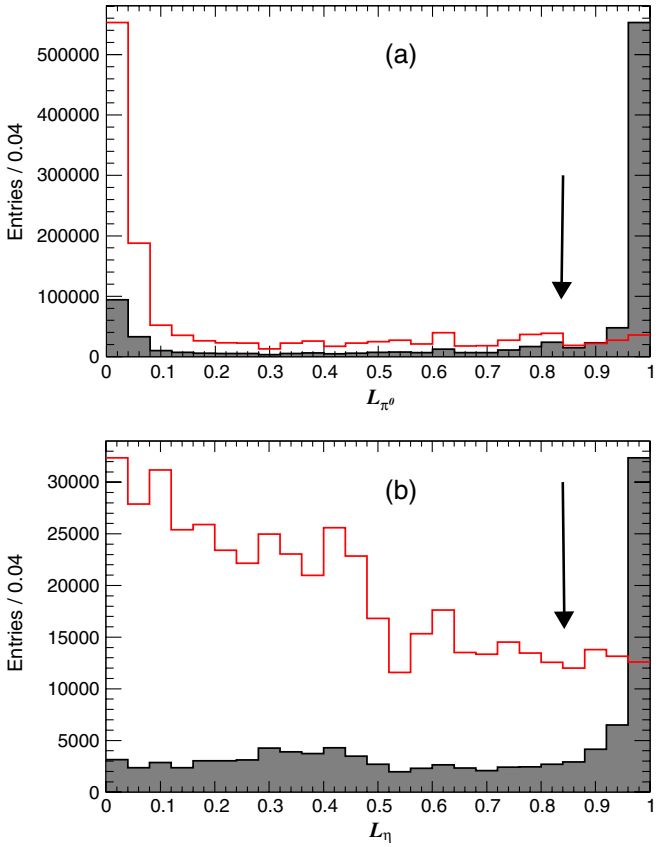

FIG. 2 (color online). (a) π^0 likelihood ratio for B candidate photons in simulated signal events (open histogram) and simulated continuum background events (shaded histogram) where the photon is required to originate from a π^0 decay. (b) η likelihood ratio for B candidate photons in simulated signal events (open histogram) and simulated continuum background events (shaded histogram) that are required to originate from an η decay. Events where both B candidate photon likelihood ratios are less than 0.84 are selected, as denoted by the arrows.

energy of the parent π^0 and will have no associated track. At a given energy, the second moment of the energy distribution around the center of the cluster will be different for a photon and a merged π^0. This allows for the construction of a quantity called the merged π^0 consistency based on the energy and second moment of the cluster. This variable compares the two inputs against known distributions from photons as well as merged π^0 decays to estimate the likelihood that the cluster originates from either source. The π^0 energy range that contributes B candidate photons in this analysis begins at about 2 GeV and extends above 6 GeV. To reduce this source of merged π^0 background, we select B candidate photons whose merged π^0 consistency is compatible with that of a photon.

In the $\Upsilon(4S)$ CM frame, the B mesons are produced nearly at rest and subsequently decay isotropically, whereas events produced in continuum processes are typically collimated in jets along the $q\bar{q}$ axis. This difference in event shape is exploited to further separate signal from continuum background events using a neural network (NN) multivariate classifier. The NN utilizes 19 input variables that characterize event level features whose distributions show separation power between signal and continuum background events. The inputs include the minimum distances between each B candidate photon EMC cluster and the EMC clusters produced by all other charged and neutral particles, respectively; this is four quantities. The inputs also include the polar angle of the B candidate momentum in the lab frame, the number of reconstructed neutral particles in the event, the number of reconstructed tracks in the event, the total missing energy, the total transverse momentum, R_2, and the event sphericity. Additionally, we include quantities that characterize the rest-of-the-event (ROE), calculated using all reconstructed particles except for one or both B candidate photons. These are: the polar angles of the event thrust axes when either B candidate photon is removed (two quantities); the first, second, and third angular moments of the event when the B candidate photon with the larger energy in the lab frame is removed; the ratio of the second-to-zeroth Fox-Wolfram moments, calculated in the CM frame, using all particles except the B candidate photon with the smaller lab energy; the second angular moment with respect to the thrust axis of the event when both B candidate photons are removed; and the event sphericity with both B candidate photons removed. We train and validate the NN using independent samples of $B^0 \to \gamma\gamma$ and continuum MC events. The training samples are constructed by first applying the photon quality, event pileup, and merged π^0 selections to the MC events. Additionally, we require $m_{\rm ES} \geq 5.2$ GeV$/c^2$ and $|\Delta E| \leq 0.5$ GeV. The surviving events are randomly divided into one set for training and one for validation. Each set contains 45 200 events where half are $B^0 \to \gamma\gamma$ MC events and the other half are continuum MC events whose composition of $e^+e^- \to q\bar{q}$ and $e^+e^- \to \tau^+\tau^-$ events is scaled to the luminosity of the on-resonance data for each component. The parameters of the NN are tuned to achieve the highest level of background rejection while avoiding overtraining the classifier. The validation sample is then used to verify its performance. The NN response is a value between 0.0 (background-like) and 1.0 (signal-like). Figure 3 shows the NN response for the validation samples for $B^0 \to \gamma\gamma$ and continuum background MC events.

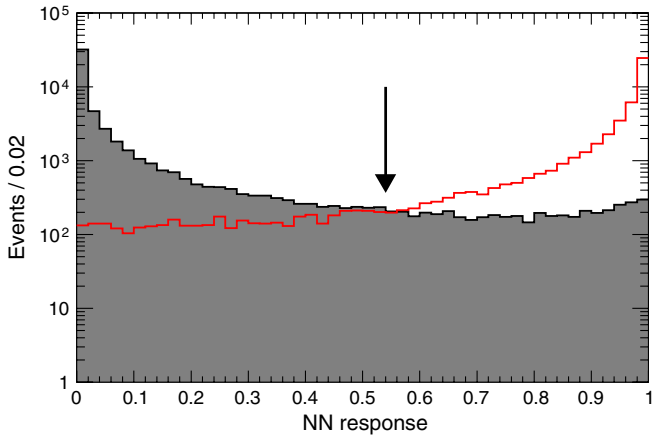

FIG. 3 (color online). Output of the neural network on the validation samples of simulated signal (open histogram) and background (shaded histogram) events. Selected events have a NN response greater than 0.54 as denoted by the arrow.

The selection criteria for L_{π^0}, L_η, the NN response, and the number of tracks are optimized using $B^0 \to \gamma\gamma$ MC events and on-resonance sideband data. The number of background events is estimated by extrapolating the sideband data into the signal region. The optimization proceeds by iterating over the space of each variable individually until we find a maximum of the figure-of-merit [15] given by the expression $\varepsilon_{\rm sig}/(3/2 + \sqrt{B})$. In this equation, $\varepsilon_{\rm sig}$ is the efficiency of the event selection derived from $B^0 \to \gamma\gamma$ MC and B is the number of background events. The iterative process continues to cycle through all variables until the selection values converge. We find the optimum values to be $L_{\pi^0} < 0.84$, $L_\eta < 0.84$, NN response greater than or equal to 0.54, and the number of tracks to be greater than two. The optimum selection criteria are found to have an overall efficiency of 26.7% on a collection of 1.96×10^6 simulated $B^0 \to \gamma\gamma$ events, while rejecting about 99.9% of background events.

B. Exclusive B decay backgrounds

Backgrounds from B decays that may peak in the $m_{\rm ES}$ and ΔE signal region are studied with large samples of simulated events. Twelve B decay modes were identified as potential background sources, and exclusive MC samples were generated for each mode. The optimized event selection is applied to each of these samples and the estimated number of background events expected in on-resonance

data are determined from the latest branching fractions [11]. After scaling the yields of these modes to the luminosity of the on-resonance data, it is estimated that they contribute a total of 1.18 ± 0.22 background events to the signal region. This number is comparable to the expected number of signal events predicted from the SM branching fraction (~ 4 events). The modes expected to contribute significantly are $B^0 \to \pi^0\pi^0$, $B^0 \to \pi^0\eta$, $B^0 \to \eta\eta$, and $B^0 \to \omega\gamma$. The $m_{\rm ES}$ distributions of these modes peak at the same value as true signal events, while the ΔE distributions peak at a value less than zero. This difference in shape of the ΔE distributions between $B^0 \to \gamma\gamma$ decays and these ''peaking'' background B decays is exploited by adding a component that describes them to the maximum likelihood function.

IV. MAXIMUM LIKELIHOOD FIT

The signal yield is extracted using a two-dimensional unbinned extended maximum likelihood (ML) fit in the region $m_{\rm ES} > 5.2$ GeV$/c^2$ and $-0.5 \le \Delta E \le 0.5$ GeV. The likelihood function for a sample of N events with signal, continuum, and peaking $B\bar{B}$ background components is given by

$$\mathcal{L} = \exp\Big(-\sum_{i=1}^{3} n_i\Big)\Big[\prod_{j=1}^{N}\Big(\sum_{i=1}^{3} n_i \mathcal{P}_i(\vec{x}_j;\vec{\alpha}_i)\Big)\Big], \qquad (3)$$

where i in this equation is an index for the three components in the fit and n_i is the event yield for each. Since the correlations between $m_{\rm ES}$ and ΔE are found to be small, the signal and continuum background PDFs, $\mathcal{P}_i$, are each defined as a product of one-dimensional PDFs in the observables $x_j \in \{m_{\rm ES}, \Delta E\}$, with parameters $\vec{\alpha}_i$. A two-dimensional histogram PDF is used for the peaking background component.

The signal PDF shapes for $m_{\rm ES}$ and ΔE are determined from simulated $B^0 \to \gamma\gamma$ events. The $m_{\rm ES}$ distribution is parameterized by a Crystal Ball function [13], and the ΔE shape is parameterized by a double-sided modified Gaussian with tail parameters given by Eq. (1). In the ML fit, the signal PDF parameters are fixed to the MC-determined values. All fixed signal parameters are later varied to evaluate the systematic uncertainty that this choice of parameterization has on the signal yield.

The continuum background $m_{\rm ES}$ distribution is parameterized by an ARGUS shape [16], while the ΔE distribution is fit with a first-order polynomial. The endpoint of the ARGUS function is fixed to the kinematic limit for B decays (5.29 GeV$/c^2$), while all other parameters are allowed to float. The PDF for the peaking background component is parameterized using large samples of simulated exclusive B decays in the form of a two-dimensional histogram PDF in $m_{\rm ES}$ and ΔE. Both the shape and yield of this component are fixed in the ML fit. The yield is fixed to 3.13 ± 0.54 events, which is the predicted number in the fit region determined from the exclusive MC studies. The fixed peaking background PDF shape and yield are later varied to evaluate the systematic uncertainty on the signal yield.

The fit is validated on an ensemble of prototype data sets whose signal and background content and shape are as expected in the on-resonance data. For the signal content, the data sets are populated with signal events assuming branching fractions of $(1, 5, 10) \times 10^{-8}$ corresponding to signal yields of 1, 6, and 12 events, respectively. Two types of data sets are constructed: one where both the signal and background events are generated by randomly sampling from their respective PDFs, and the other where the background events are generated from a random sampling of the background PDF while the signal events are embedded

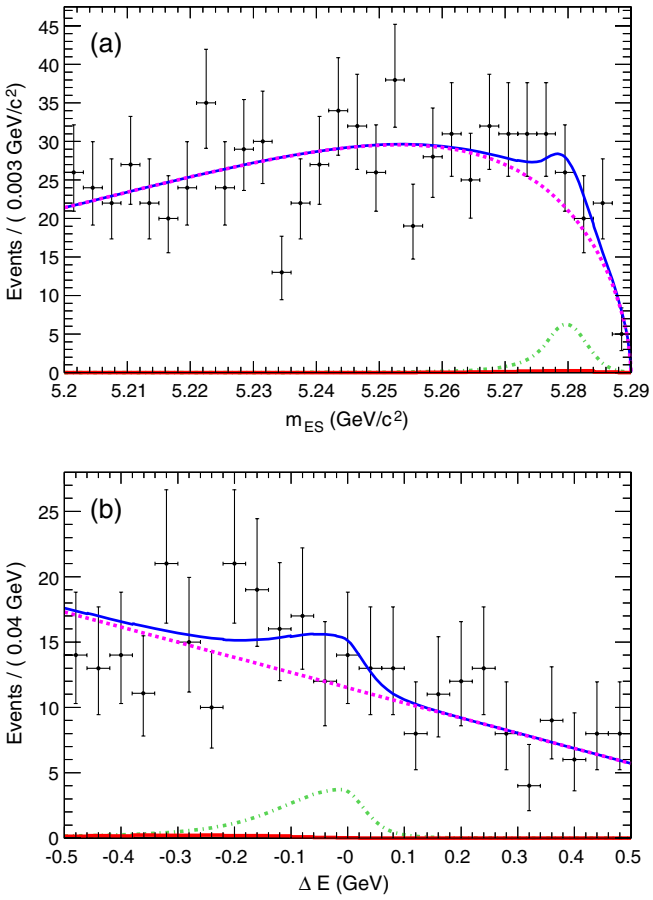

FIG. 4 (color online). Projections of the ML fit onto $m_{\rm ES}$ and ΔE. (a) The projection of the $m_{\rm ES}$ component when the range of ΔE has been restricted to $-0.30 \le \Delta E \le 0.13$ GeV. (b) The ΔE projection of the fit when the range of $m_{\rm ES}$ has been restricted to $m_{\rm ES} > 5.27$ GeV$/c^2$. The points represent the on-resonance data. The solid curve represents the total PDF, the dashed curve is the continuum background component, the dot-dashed curve is the signal component, and the long-dashed curve is the peaking background component. With an expected yield of approximately one event, the peaking background component is nearly indistinguishable from the x axis.

directly from the simulated signal data set. The results of the validation studies were consistent with negligible bias in the fit result for the signal yield.

The on-resonance $\Upsilon(4S)$ data contains 1679 events after the optimized event selection criteria are applied. We perform the ML fit to extract the signal yield and find $N_{\rm sig} = 21.3^{+12.8}_{-11.8}$ events corresponding to a statistical significance of 1.8σ. The significance is computed as $\sqrt{2 \cdot \Delta \ln \mathcal{L}}$, where $\Delta \ln \mathcal{L}$ is the difference in the log-likelihood between the best fit to on-resonance data and a fit where the signal yield is fixed to zero. Figure 4 shows projections of the PDF components from the ML fit. For the $m_{\rm ES}$ projection, the range of ΔE has been restricted to $-0.30 \leq \Delta E \leq 0.13$ GeV. For the ΔE projection, the range of $m_{\rm ES}$ is restricted to $m_{\rm ES} > 5.27$ GeV$/c^2$.

Since the signal yield extracted from the ML fit is outside the range initially tested during the fit validation, we subsequently ran additional validation studies with input signal yields up to twice the fit result. We observed a small fit bias, which we estimate to be 0.5 ± 0.1 events when the input signal equals the result of our fit. Consequently, we subtract this bias from our fit result, giving a corrected signal yield of $20.8^{+12.8}_{-11.8}$ events.

V. SYSTEMATIC UNCERTAINTIES

Systematic errors that affect the calculation of the branching fraction are investigated and include uncertainties on the number of $B^0\bar{B}^0$ events in the data set, signal efficiency, and the signal yield from the fit. Differences between data and MC can lead to an error on the derived signal efficiency. The identified sources that can lead to this error include uncertainties in tracking, track multiplicity, photon reconstruction, the L_{π^0} and L_η requirements, and the NN selection. The uncertainties in the modeling of the signal and $B\bar{B}$ background shapes in the maximum likelihood fit can also affect the uncertainty on the signal yield.

The systematic error associated with counting the number of $B\bar{B}$ pairs in the data set is 1.1%. The number of $B^0\bar{B}^0$ pairs is obtained by multiplying the $\Upsilon(4S) \to B^0\bar{B}^0$ branching fraction, equal to $(48.4 \pm 0.6)\%$ [11], with the total number of $B\bar{B}$ pairs, from which a systematic error of 1.7% is assigned. A study of the track finding inefficiency results in an assignment of a 0.2% systematic uncertainty for the selection of events with at least three reconstructed tracks. The uncertainty in the signal efficiency due to the requirement of at least three reconstructed charged tracks is estimated to be 3.4%, including components for both generator-level simulation errors and detector-associated data versus MC differences. The efficiencies in data and MC for detecting high-energy photons which pass the selection criteria (including the merged π^0 consistency) were compared using a sample of $e^+e^- \to \mu^+\mu^-\gamma$ events with the photon energy in the CM frame restricted to be consistent with the energy of $B^0 \to \gamma\gamma$ photons. No significant difference is observed. An uncertainty of 2% per photon is assigned to account for possible data versus MC differences due to the required minimum distance between the candidate photon cluster and all other clusters, based on a study that embedded high-energy photons in both data and MC events. We combine this uncertainty linearly for both photons in $B^0 \to \gamma\gamma$ and assign an overall photon efficiency systematic of 4%. The cluster time selection is compared in data and MC and we assign a systematic uncertainty of 0.7% for each B candidate. The systematic uncertainty due to the π^0 and η likelihood ratios is estimated to be 1.0% for each, based on a study that embedded signal-like photons in data and MC events in which one B meson was fully reconstructed in the decay $B \to D\pi$. The signal efficiencies for the L_{π^0} and L_η selections for data and MC are calculated by pairing the embedded signal-like photon with all other photons in these events that are not associated with the reconstructed B. The systematic uncertainty due to the NN is estimated by comparing the efficiencies of data to MC in signal-like events. Signal-like events are selected by applying all event selection criteria, but reversing either the NN, the L_{π^0} or the L_η selection for one of the B candidate photons. The efficiencies are then calculated from events in the fit region with the signal region excluded. For all selection reversal scenarios, the ratio of the efficiencies is found to be consistent with unity and has a typical statistical error of 3.0%, which is taken as the systematic uncertainty.

The systematic uncertainty on the signal yield due to the choice of fit model has five components. The first is due to the fixed signal shape for the $m_{\rm ES}$ and ΔE PDFs. To estimate the systematic uncertainty related to this choice of parameterizations, the fixed parameters are varied within their $\pm 1\sigma$ errors, the on-resonance data set is refit, and the change in the signal yield is calculated for each parameter. The total systematic uncertainty is taken to be the sum in quadrature of all variations and is found to be 0.6 events. A comparison between photon response in $e^+e^- \to \mu^+\mu^-\gamma$ events in data and MC, using photons in the energy range relevant to the decay $B^0 \to \gamma\gamma$, shows that the size of the variation in the signal shape parameters is sufficient to take into account any systematic effects from parameterizing the signal PDF shapes from MC. The second component is due to the parameterization choice for the signal shape. While the PDF used to fit the $m_{\rm ES}$ distribution replicates the shape in $B^0 \to \gamma\gamma$ MC, there is a slight disagreement between the ΔE distribution in $B^0 \to \gamma\gamma$ MC and that of the double-sided modified Gaussian used to describe it, Eq. (1). To test how large of an effect this difference may have on the signal yield, the ΔE distribution is parameterized using a Crystal Ball shape [13] that provides a larger discrepancy from the MC shape. Ensembles of simulated experiments are performed wherein each experiment consists of an independent data set fit first using the ΔE parameterization described in

Sec. IV and then using the alternative parameterization described here. The signal yields for each fit are compared and the average difference is found to be 0.2 events which is assigned as the systematic uncertainty. The third component is due to the choice of the ΔE continuum background shape. Repeating the fit to data using a second-order polynomial for ΔE results in an increase of 1.9 events in the signal yield, which we take to be the systematic error for this component. The fourth component is due to the choice of shape and normalization for the peaking background PDF, both of which are fixed in the ML fit. The shape is fixed from the $m_{\rm ES}$ and ΔE distributions of simulated exclusive B decays, while the yield is fixed to the expected number of events in on-resonance data. To estimate the systematic uncertainty on the signal yield, both the peaking background yield and shape are varied. The uncertainties on the yields of the individual peaking background modes are added linearly to determine the uncertainty on the total yield of the peaking component in the ML fit. This results in a range for the peaking yield between 2.02 and 4.24 events. The shape of the peaking PDF is varied by replacing it solely with the shape derived from $B^0 \to \pi^0\pi^0$ MC. The ΔE distribution of this mode most closely resembles that from $B^0 \to \gamma\gamma$ MC. Another ensemble of simulated experiments were performed where the differences in the signal yield were compared when using these set of extreme variations in the peaking component and those from the ML fit to data. We take the maximal change in the signal yield and assign a conservative systematic uncertainty of 0.5 events. The fifth component is due to the fit bias found from an ensemble of simulated prototype data sets. We take half the bias and assign it as a systematic uncertainty of 0.25 events. The five components are added in quadrature to give a systematic uncertainty for the ML fit of 2.1 events corresponding to 9.9%.

These results are added in quadrature to give a total systematic uncertainty on the signal yield of 2.6 events, corresponding to 12.1%. The separate contributions to the systematic uncertainty are summarized in Table I.

TABLE I. Summary of the systematic uncertainties expressed as a percent of the signal yield.

Source	Uncertainty on $N_{\rm sig}$ (%)
$B^0\bar{B}^0$ counting	1.7
Tracking efficiency	0.2
Track multiplicity	3.4
Photon efficiency	4.0
Cluster time	0.7
L_{π^0} and L_η	2.8
Neural network	3.0
Fit uncertainty	9.9
Sum in quadrature	12.1

VI. RESULTS

The branching fraction is calculated from the measured signal yield using

$$\mathcal{B}(B^0 \to \gamma\gamma) = \frac{N_{\rm sig}}{\varepsilon_{\rm sig} \cdot 2 \cdot N_{B^0\bar{B}^0}}, \quad (4)$$

where $N_{\rm sig}$ is the signal yield from the maximum likelihood fit, $\varepsilon_{\rm sig}$ is the signal selection efficiency determined from simulated $B^0 \to \gamma\gamma$ events, and $N_{B^0\bar{B}^0}$ is the number of neutral B meson pairs in the on-resonance data set. We calculate the branching fraction to be

$$\mathcal{B}(B^0 \to \gamma\gamma) = (1.7 \pm 1.1 \pm 0.2) \times 10^{-7}, \quad (5)$$

with a statistical significance of 1.8σ, where the first error is statistical and the second is systematic.

The upper limit at the 90% CL is obtained by integrating the likelihood curve resulting from the ML fit from zero to the value of $N_{\rm sig}$ which contains 90% of the area under the curve. To incorporate the systematic uncertainty into the determination of the upper limit, the likelihood curve is convolved with a Gaussian shape whose width is equal to the total systematic uncertainty of 2.6 events. This yields a value of $N_{\rm sig} = 39$ events corresponding to an upper limit of

$$\mathcal{B}(B^0 \to \gamma\gamma) < 3.2 \times 10^{-7}\ (90\%\text{CL}). \quad (6)$$

Figure 5 shows the likelihood curve from the fit after convolution with the Gaussian shape. The shaded region corresponds to the 90% integral of the curve.

This limit is nearly a factor of 2 below the best previous upper limit of $\mathcal{B}(B^0 \to \gamma\gamma) < 6.2 \times 10^{-7}$ set by Belle [4], and is consistent with the SM branching fraction. This limit

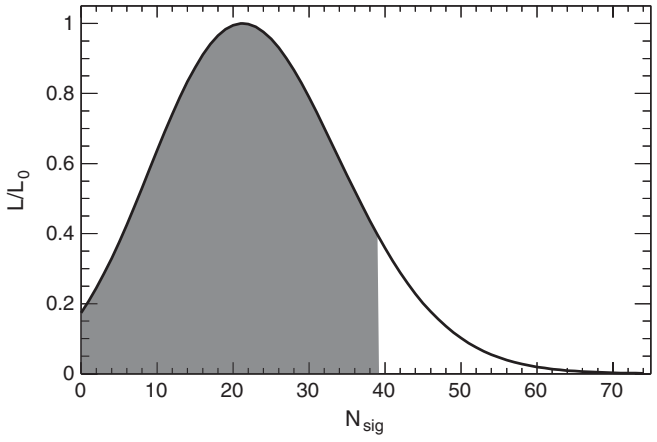

FIG. 5. Likelihood curve from the maximum likelihood fit, as a function of the signal yield, after convolution with a Gaussian shape whose width is equal to the total systematic error. The shaded region corresponds to the integral of the curve up to 90% of its total area. The y axis, L/L_0, is the ratio of the likelihood function for a given $N_{\rm sig}$ to the maximum likelihood.

may allow tighter constraints on models that incorporate physics beyond the SM.

ACKNOWLEDGMENTS

We are grateful for the extraordinary contributions of our PEP-II colleagues in achieving the excellent luminosity and machine conditions that have made this work possible. The success of this project also relies critically on the expertise and dedication of the computing organizations that support *BABAR*. The collaborating institutions wish to thank SLAC for its support and the kind hospitality extended to them. This work is supported by the US Department of Energy and National Science Foundation, the Natural Sciences and Engineering Research Council (Canada), the Commissariat à l'Energie Atomique and Institut National de Physique Nucléaire et de Physique des Particules (France), the Bundesministerium für Bildung und Forschung and Deutsche Forschungsgemeinschaft (Germany), the Istituto Nazionale di Fisica Nucleare (Italy), the Foundation for Fundamental Research on Matter (The Netherlands), the Research Council of Norway, the Ministry of Education and Science of the Russian Federation, Ministerio de Ciencia e Innovación (Spain), and the Science and Technology Facilities Council (United Kingdom). Individuals have received support from the Marie Curie IEF program (European Union), the A. P. Sloan Foundation (USA) and the Binational Science Foundation (USA-Israel).

[1] S. W. Bosch and G. Buchalla, J. High Energy Phys. 08 (2002) 054.
[2] T. M. Aliev and E. O. Iltan, Phys. Rev. D **58**, 095014 (1998).
[3] A. Gemintern, S. Bar-Shalom, and G. Eilam, Phys. Rev. D **70**, 035008 (2004).
[4] S. Villa *et al.* (Belle Collaboration), Phys. Rev. D **73**, 051107 (2006).
[5] J. Wicht *et al.* (Belle Collaboration), Phys. Rev. Lett. **100**, 121801 (2008).
[6] B. Aubert *et al.* (*BABAR* Collaboration), Nucl. Instrum. Methods Phys. Res., Sect. A **479**, 1 (2002).
[7] M. Kocian (*BABAR* Collaboration), Report No. SLAC-PUB-10170, 2002.
[8] D. Lange, Nucl. Instrum. Methods Phys. Res., Sect. A **462**, 152 (2001).
[9] T. Sjostrand, Comput. Phys. Commun. **82**, 74 (1994).
[10] S. Agostinelli *et al.* (GEANT4 Collaboration), Nucl. Instrum. Methods Phys. Res., Sect. A **506**, 250 (2003).
[11] K. Nakamura *et al.* (Particle Data Group), J. Phys. G **37**, 075021 (2010).
[12] G. C. Fox and S. Wolfram, Phys. Rev. Lett. **41**, 1581 (1978).
[13] J. E. Gaiser *et al.*, Phys. Rev. D **34**, 711 (1986).
[14] A. Drescher *et al.* (ARGUS Collaboration), Nucl. Instrum. Methods Phys. Res., Sect. A **237**, 464 (1985).
[15] G. Punzi, arXiv:physics/0308063v2.
[16] H. Albrecht *et al.* (ARGUS Collaboration), Z. Phys. C **48**, 543 (1990).